Analytical Chemistry: A Journal (2024)
Clausius Scientific Press, Canada

DOI: 10.23977/analc.2024.030111
ISSN 2616-1958 Vol. 3 Num. 1

Colorimetric Detection of Alkaline Phosphatase (ALP) Based on Fe_3O_4@MIL@Pt

Bing Li[1,a,*]

[1]*School of Chemistry, South China Normal University, Guangzhou, Guangdong, China*
[a]*bingli0623@163.com*
[*]*Corresponding author*

Keywords: Fe_3O_4@MIL@Pt; colorimetric method; 3,3',5,5'-Tetramethylbenzidine (TMB); ascorbic acid (AA); alkaline phosphatase (ALP)

Abstract: This study presents an advanced colorimetric biosensor based on Fe_3O_4@MIL@Pt nanocomposites for the sensitive and selective quantification of alkaline phosphatase (ALP). The nanocomposite system combines the catalytic capabilities of Fe_3O_4 nanoparticles, the structural advantages of metal-organic frameworks (MIL), and the catalytic prowess of platinum (Pt) nanoparticles. Through the implementation of a triple signal amplification strategy, the catalytic efficiency of TMB oxidation is significantly boosted, resulting in a distinct blue color development of the oxidized TMB (OX-TMB). The assay is designed such that AA reduces OX-TMB, leading to a measurable decrease in absorbance, while ALP activity is reflected in the hydrolysis of ascorbic acid-2-phosphate (AA2P) to AA, thereby modulating the colorimetric signal. This system allows for highly sensitive detection of ALP by monitoring absorbance changes. The analytical performance is characterized by a detection limit of 0.091 mU/mL with a linear range from 0.5 to 10 mU/mL. Importantly, the method demonstrates excellent analytical performance with real serum samples, emphasizing its potential for clinical diagnostic applications.

1. Introduction and Background

Alkaline phosphatase (ALP) is a key enzyme in phosphate metabolism, widely found in various tissues and biological fluids. It catalyzes the hydrolysis and dephosphorylation of proteins, nucleic acids, and small molecule phosphates [1]. ALP levels in adult serum typically range from 40 to 190 U/L but can rise to 500 U/L during pregnancy or in pediatric populations [2]. Abnormal ALP levels are associated with several pathological conditions [3-5]. In clinical practice, ALP activity is a significant biomarker for diseases like osteoporosis, biliary obstruction, and cancers such as ovarian and prostate cancer [6]. Therefore, sensitive and accurate ALP detection methods are crucial for clinical diagnostics.

Various methods for ALP detection have been developed, including electrochemical sensors [7,8], electrochemiluminescence [9,10], surface-enhanced Raman scattering [11,12], and colorimetric and fluorescence assays [13]. However, many face challenges like low sensitivity or complex instrumentation. Colorimetric assays, known for their simplicity and affordability, often require hazardous organic substrates [14,15]. This highlights the need for a simple, sensitive, and safe ALP

detection method. The study of nanozymes, nanomaterials with enzymatic activity, has gained attention [16-19]. These catalysts outperform natural enzymes by offering controlled synthesis, cost-efficiency, structural flexibility, and high stability [20-22]. Their performance arises from combining catalytic functions with nanomaterial properties like magnetism and photothermal effects, enabling multifunctionality [23]. Nanozymes mimic the kinetic behavior of natural enzymes under mild conditions [24-25]. In 2007, Fe_3O_4 nanoparticles' peroxidase-like activity was discovered [26], but their low catalytic efficiency and color intensity limit detection sensitivity [27]. To improve this, advanced nanozymes, including metal nanoparticles [28], oxides [29], sulfides [30], carbon-based materials [31], and MOFs [32], have been developed. Multifunctional nanozyme composites show potential for enhancing biosensor performance [33]. Nanozymes offer high stability, economic efficiency, biocompatibility, large surface areas, and tunable properties, making them ideal for diverse applications [34]. Core-shell nanozymes, with controlled size and surface characteristics, enhance catalytic efficiency and selectivity, broadening their analytical applications [35-36].

The Fe_3O_4@MIL@Pt-based colorimetric platform enhances sensitivity and reliability through its advanced composite design. By combining Fe_3O_4's magnetic properties, MIL's large surface area with active sites, and Pt's catalytic efficiency, the platform maximizes synergistic effects for optimized analysis. Fe_3O_4 aids in efficient separation, MIL boosts catalytic activity, and Pt amplifies detection signals, creating a robust system. This simple, cost-effective platform operates without complex instruments, making it ideal for clinical diagnostics and applications in environmental, toxicological, and food safety fields. Its effectiveness in real-world samples demonstrates its practicality and accuracy in complex matrices.

The platform detection strategy is shown in Figure 1. The synthesized core-shell nanoenzyme with peroxidase like activity can oxidize TMB to produce blue OX-TMB, and the stronger the enzyme activity, the darker the oxidation color. At the same time, ALP can catalyze AA2P to produce ascorbic acid AA with reducing properties, which can reduce OX-TMB to colorless TMB. The degree of reduction is related to the activity of ALP.

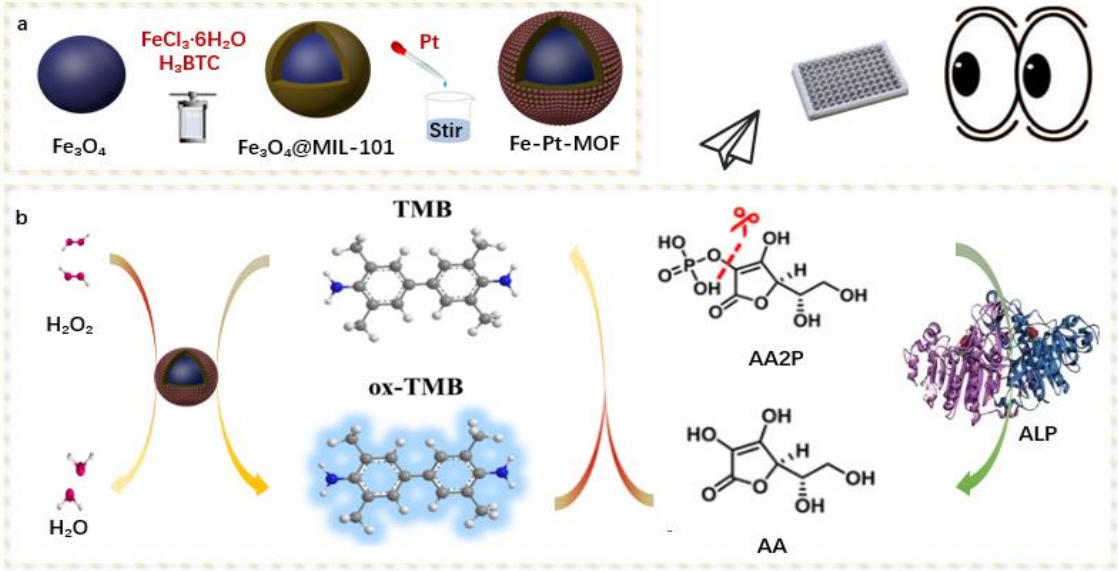

Figure 1: Experimental schematic diagram

2. Experimental Section

2.1. Chemicals

The Fe_3O_4@MIL@Pt nanocomposites were synthesized using high-purity chemicals. Ferric chloride hexahydrate ($FeCl_3$ $6H_2O$), ethylene glycol ($C_2H_6O_2$), and N,N-dimethylformamide (C_3H_7NO) were obtained from Tianjin Damo Chemical Reagent Factory. Sodium citrate ($C_6H_5Na_3O_7$), urea (CH_4N_2O), trimesic acid (H_3BTC), 2-amino-2-methyl-1-propanol ($C_4H_{11}NO$), and other reagents, including ascorbic acid 2-phosphate (AA2P) and alkaline phosphatase, were purchased from Shanghai Macklin Biochemical Technology Co., Ltd. 3,3',5,5'-Tetramethylbenzidine (TMB) and sodium hexachloroplatinate hexahydrate were sourced from Shanghai Aladdin Biochemical Technology Co., Ltd. Ethanol was supplied by Tianjin Zhiyuan Chemical Reagent Co., Ltd., and standard solutions of Na, Cl, Ca, and NO_3 were from the Beijing Nonferrous Metals Research Institute. Hydrogen peroxide (30%) and deionized water were procured through the university's procurement system and Yibao Co., Ltd., respectively. All chemicals were of analytical grade and used without further purification.

2.2. Equipment and Instruments

In this study, we used advanced instruments for synthesizing, characterizing, and analyzing Fe_3O_4@MIL@Pt nanocomposites:

- TLE204E Electronic Balance (Mettler-Toledo) for precise mass measurements.
- RET control-visc Multifunctional Thermostatic Magnetic Stirrer (IKA) for controlled mixing.
- HC-2518R High-Speed Refrigerated Centrifuge (Anhui Zhongke) for rapid sample separation.
- KQ-300DE Digital Ultrasonic Cleaner (Kunshan Ultrasonic) for thorough cleaning.
- Zetasizer Nano ZS90 (Malvern Instruments) for nanoparticle size and Zeta potential analysis.
- Spectrum Two FT-IR Spectrometer (PerkinElmer) for chemical composition analysis.
- Ultima IV X-Ray Diffractometer (Rigaku) for crystalline structure determination.
- K-Alpha XPS (Thermo Fisher) for surface chemistry analysis.
- Centrifuge 5418R (Eppendorf) for sample preparation and purification.
- BPZ-6033 Vacuum Drying Oven (Shanghai Yiheng) for sample drying.
- WGL-65B Electric Blast Drying Oven (Tianjin Tailor) for rapid dehydration.
- Vortex-Genie 2 Vortex Mixer (Scientific Industries) for reagent mixing.
- SuperMax 3100 Microplate Reader (Shanghai Flash Biotech) for absorbance and fluorescence measurements.
- ZEISS Ultra 55 FE-SEM (Carl Zeiss) for high-resolution imaging.

2.3. Synthesis of Fe_3O_4@MIL@Pt Nanomaterials

The Fe_3O_4@MIL@Pt nanocomposites were prepared following established methods. Fe_3O_4 nanoparticles were first synthesized via a solvothermal process. A solution of 2.06 g sodium citrate (8 mmol), 0.72 g urea (12 mmol), and 1.08 g ferric chloride hexahydrate (4 mmol) in 50 mL ethylene glycol was mixed with 600 mg of 50% polyacrylamide. After stirring to form a uniform greenish solution, the mixture was heated in a Teflon-lined autoclave at 200°C for 8 hours. The resulting black nanoparticles were washed with ethanol and water, then vacuum-dried at 60 ℃ for 24 hours.

The Fe_3O_4 nanoparticles served as cores for the in situ synthesis of MIL-101(Fe) MOF layers, optimized with x/y molar ratios of 11:2 and 5:2. Finally, ~6.5 nm Pt nanoparticles were anchored onto the Fe_3O_4@MIL surface via strong coordination interactions, yielding Fe_3O_4@MIL@Pt

nanocomposites with superior catalytic properties.

2.4. Assessment of Peroxidase-Like Activity of Fe_3O_4@MIL@Pt

In this study, we evaluated the peroxidase-like activity of Fe_3O_4@MIL@Pt nanocomposites using three distinct colorimetric substrates—TMB, ABTS, and OPD, each at a concentration of 2.9 mM. The experiments involved mixing 50 µL of each substrate with 50 µL of hydrogen peroxide (5 mM), 5 µL of Fe_3O_4@MIL@Pt suspension (5 µg·mL^{-1}; with a molar ratio of Fe_3O_4 to MIL of 11:2), and 95 µL of acetate buffer (pH 4.5, 0.2 M). After a 3-minute reaction period, absorbance measurements were conducted using a multifunctional microplate reader. The results indicated that Fe_3O_4@MIL@Pt exhibited significant peroxidase-like activity, with TMB showing the most favorable characteristics due to its lower toxicity, leading to its selection as the substrate for subsequent experiments.

2.5. Steady-State Kinetic Studies

$$\frac{1}{v} = \frac{K_m}{V_{max}} \cdot \frac{1}{[S]} + \frac{1}{V_{max}} \quad (1)$$

The initial reaction rate (V) was determined as a function of substrate concentration [S], with Vmax as the endpoint. To study the inhibitory effect of ascorbic acid (AA) on 3,3',5,5'-tetramethylbenzidine (TMB) oxidation, a reaction mixture containing 10 µL of 40 µM AA, 50 µL of 5 mM hydrogen peroxide, 50 µL of 5 mM TMB, 5 µL of 5 µg·mL^{-1} Fe_3O_4@MIL@Pt, and 85 µL of acetate buffer was incubated at 25°C for 10 minutes. UV-visible spectrophotometry using a multifunctional microplate reader assessed TMB oxidation. To optimize ascorbic acid 2-phosphate (AA2P) conditions, varying AA2P concentrations (0-200 µM·L^{-1}) were incubated with 20 mU·mL^{-1} alkaline phosphatase (ALP) in AMP buffer (pH 3-11, 0.1 M) at 37°C for 20 minutes, allowing determination of the optimal pH and substrate concentration. For ALP assays, 20 µL of pH 11 AMP buffer was combined with 5 µL of 90 µM AA2P and 5 µL of ALP (0-30 µM). After a 20-minute incubation at 37 ℃ for AA2P hydrolysis, 5 µL each of 5 mM hydrogen peroxide, 5 mM TMB, 5 µg·mL^{-1} Fe_3O_4@MIL@Pt, and 130 µL of pH 9 acetate buffer were added to initiate the colorimetric reaction. Absorbance changes at 652 nm were measured, demonstrating the Fe_3O_4@MIL@Pt nanocomposites' catalytic efficiency for ALP detection. This optimized platform ensures Fe_3O_4@MIL@Pt's effective use for sensitive and selective ALP detection, with accurate AA2P conditions and reliable absorbance measurements facilitated by a multifunctional microplate reader.

3. Results and Discussion

3.1. Representation Fe_3O_4@MIL@Pt

The preparation of Fe_3O_4@MIL@Pt nanocomposites was achieved through a hydrothermal process, as depicted in Figure 2A. We conducted a comprehensive characterization of the synthesized nanocomposites using a suite of analytical techniques. Scanning electron microscopy (SEM) and X-ray powder diffraction (XRD) provided insights into the morphology and crystalline structure, respectively. Fourier-transform infrared spectroscopy (FT-IR), X-ray photoelectron spectroscopy (XPS), and Zeta potential measurements further elucidated the chemical composition and surface charge properties of the material.

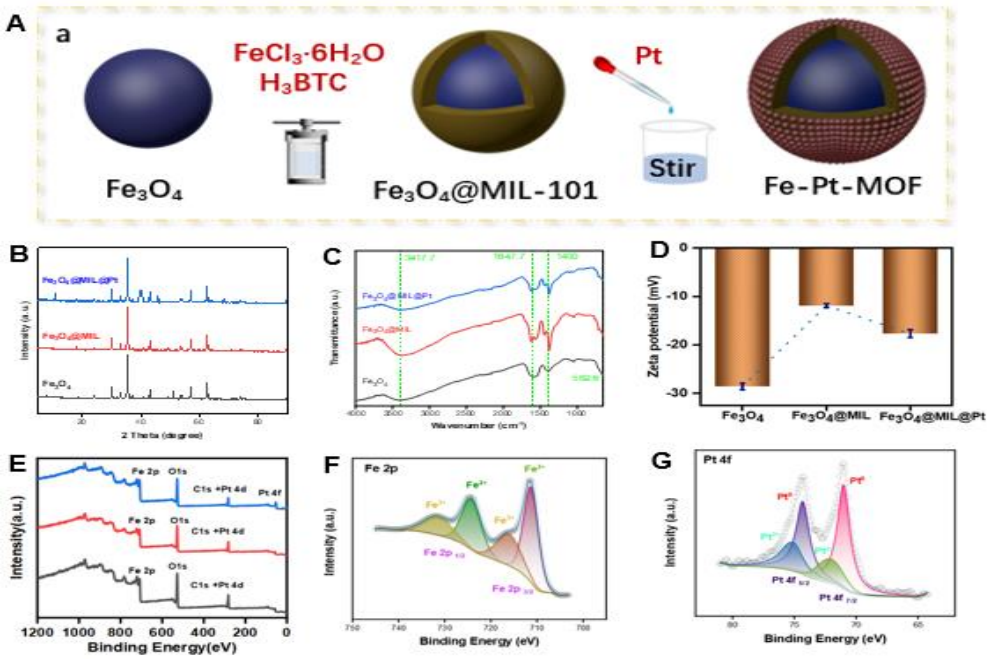

Figure 2: (A) Experimental schematic diagram (B)XRD (C)FT-IR (D)Zeta (E)XPS (F)Fe 2p (G)Pt4f

The XRD pattern in Figure 2B confirms the synthesis of Fe_3O_4, with distinct peaks for the (220) and (311) planes. The intensified peaks, along with the peak at $2\theta = 38°$, signify successful deposition of the MIL layer and Pt nanoparticles. FT-IR spectra (Figure 2C) highlight Fe-O bonds with absorption bands at 3417.7 cm^{-1} and 582.6 cm^{-1}, while peaks at 1400 cm^{-1} and 1647.7 cm^{-1} confirm Pt binding to the Fe_3O_4@MIL surface. Zeta potential analysis (Figure 2D) reveals significant surface charge changes: the MIL layer increases Zeta potential, while Pt incorporation decreases it, confirming successful layer assembly. XPS analysis (Figure 2E) identifies Fe, O, Pt, and C as key elements, with binding energies at 710.1 eV (Fe 2p), 530.9 eV (O 1s), 335.1 eV (Pt 4f), and 284.4 eV (C 1s). High-resolution XPS for Fe 2p (Figure 2F) shows peaks at 724.6 eV and 711.4 eV (Fe^{2+}), alongside peaks at 716.4 eV and 732 eV for Fe^{3+}, indicating a mixed-valence state that influences catalytic properties. The Pt 4f spectrum (Figure 2G) displays characteristic peaks for Pt 4f 5/2 and Pt 4f 7/2, confirming Pt incorporation critical for enhanced catalysis. The shifts in Zeta potential align with the successful assembly of MIL and Pt layers on the Fe_3O_4 core, reflecting changes in surface composition. XPS confirms the incorporation of Fe, O, Pt, and C in expected chemical states, validating the synthesis process and highlighting the material's advanced catalytic and sensing capabilities.

3.2. Enzymatic Activity of Fe_3O_4@MIL@Pt

When H_2O_2 was introduced, the Fe_3O_4@MIL@Pt nanocomposites efficiently facilitated the oxidation of the colorimetric substrates TMB, ABTS, and OPD. This catalytic action resulted in the distinct colors blue, green, and yellow, corresponding to each substrate. The UV-Vis spectroscopy analysis confirmed these observations, with the appearance of specific absorption peaks at 416 nm, 448 nm, and 652 nm for TMB, ABTS, and OPD, respectively (as shown in Figure 3). These findings highlight the robust peroxidase-like activity of the Fe_3O_4@MIL@Pt nanocomposites.

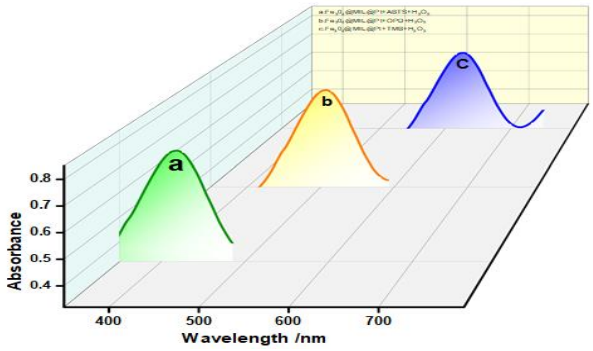

Figure 3: Enzyme Activity Exploration

To refine the catalytic performance of Fe_3O_4@MIL@Pt within the TMB-H_2O_2 colorimetric system, a systematic investigation into the influence of pH and temperature was conducted. As depicted in Figures 4A and 4B, the catalytic activity initially increased, reaching an optimum at pH 5, beyond which it declined across the pH range of 2.0 to 8.0. Temperature also played a significant role, with activity escalating from 10 ℃ to 40 ℃ and peaking at 25 ℃, after which it diminished with further temperature elevation. These observations establish pH 5 and 25 ℃ as the optimal conditions for achieving peak catalytic efficiency, setting the stage for subsequent experimental protocols.

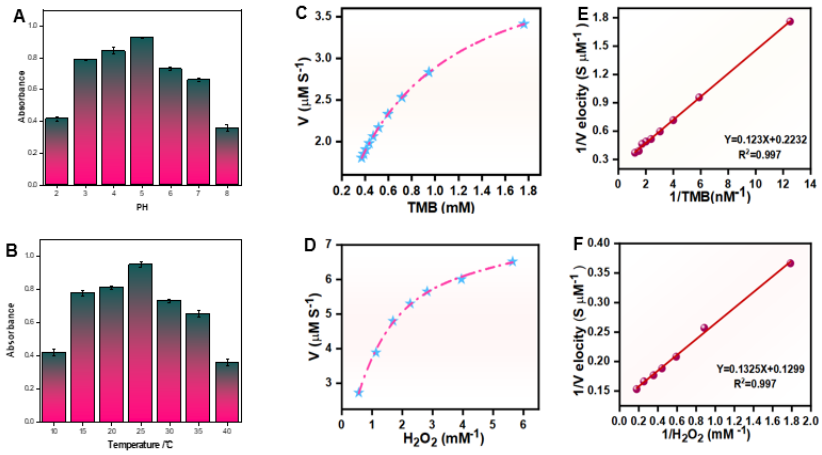

Figure 4: (A)PHand(B) Temperature (C) enzyme kinetics plot and (E)Lineweaver-Burk plot of Fe_3O_4@MIL@Pt on substrate TMB; (D) enzyme kinetics and (F)Lineweaver-Burk plots of Fe_3O_4@MIL@Pt on substrate H_2O_2;

In enzyme kinetics research, we explored the catalytic characteristics of Fe_3O_4@MIL@Pt by varying one substrate's concentration while keeping the other constant. The results showed that the catalytic behavior followed the Michaelis-Menten kinetic model within a specific range, as seen in Figures 4C and 4D. Using the Lineweaver-Burk plot, we determined the Michaelis constant (Km) and maximum reaction rate (Vmax), revealing a clear linear relationship. These findings validate the nanozyme's adherence to Michaelis-Menten kinetics and provide insights into its enzymatic properties. The results confirm the catalytic efficiency of Fe_3O_4@MIL@Pt nanocomposites and their potential to mimic enzymatic reactions. This study enhances understanding of their catalytic mechanisms and offers valuable reference data for designing advanced biosensors.

$$\frac{1}{v} = \frac{K_m}{V_{max}} \cdot \frac{1}{[S]} + \frac{1}{V_{max}} \quad (2)$$

Within the kinetic analysis, the variable v signifies the initial reaction velocity at different

substrate concentrations, with [S] representing the substrate concentration. The Michaelis constant (Km) is the concentration of substrate at which the reaction rate is half of Vmax, the maximum reaction velocity. This constant serves as a pivotal indicator of the enzyme's affinity for its substrate; a lower Km indicates a greater affinity.

In the case of the TMB substrate, the Michaelis constant (Km) for Fe_3O_4@MIL@Pt is determined to be 0.551 mmol/L, with a maximum reaction rate (Vmax) of 4.48 $\times 10^{-8}$ mol/s. When H_2O_2 serves as the substrate, the Km is found to be 1.02 mmol/L, and the Vmax is 7.7 $\times 10^{-8}$ mol/s. Notably, the affinity of Fe_3O_4@MIL@Pt for TMB, as indicated by its Km, is on par with that of natural horseradish peroxidase, which has a Km of 0.434 mmol/L. However, Fe_3O_4@MIL@Pt demonstrates a considerably higher affinity for H_2O_2, with its Km being significantly lower than that of horseradish peroxidase, which is 3.7 mmol/L.

3.3. Detection Results for ALP

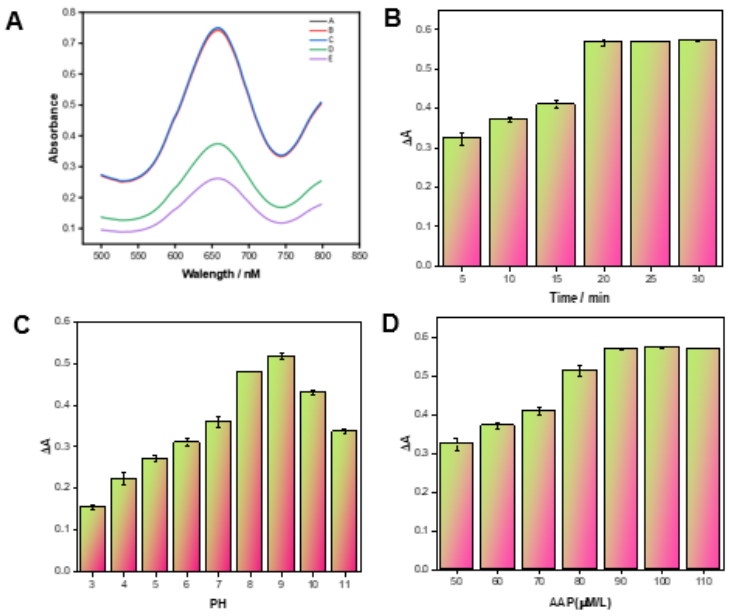

Figure 5: (A)feasibility testing (B)(C)and(D)PH,Time,AA2P optimization

In the initial phase of our study, we evaluated the Fe_3O_4@MIL@Pt system's efficacy for detecting alkaline phosphatase (ALP). Preliminary experiments showed significant changes in the color and absorbance of the oxidized 3,3',5,5'-tetramethylbenzidine (oxTMB) solution upon introducing ALP and ascorbic acid 2-phosphate (AA2P). Increasing ALP concentrations caused reduced absorbance and visible lightening, as shown in Figure 5A, curves d and e. This confirms ALP catalyzes AA2P into ascorbic acid (AA), which reduces oxTMB, demonstrating the system's ALP sensitivity.

In contrast, isolated use of ALP or AA2P caused minimal absorbance changes (curves b and c), highlighting their interdependence for oxTMB reduction. The data indicate that higher ALP activity decreases oxTMB absorbance, lightening the solution, with AA production increasing proportionally to both AA2P concentration and ALP activity.

The detection of ALP activity with high sensitivity and over an appropriate linear range is contingent upon the substrate concentration and the reaction duration. Our study optimized these parameters by assessing the impact of varying AA2P concentrations on the absorbance at 652 nm (ΔA652 nm), under conditions that included a fixed pH and a defined period for ALP-catalyzed

hydrolysis. The results in Figure 5indicated an increment in ΔA652 nm with increasing AA2P concentrations, reaching an optimum at 90 μmol/L. Beyond this concentration, no significant changes in absorbance were observed, suggesting a saturation point. Thus, an AA2P concentration of 90 μmol/L was identified as optimal for achieving the most sensitive and effective ALP activity detection.

In our investigation into the kinetics of the reaction, we observed that the absorbance change at 652 nm (ΔA652 nm) escalated with extended reaction times, stabilizing after a 20-minute incubation period. This plateau suggests that the catalytic hydrolysis of ascorbic acid 2-phosphate (AA2P) by alkaline phosphatase (ALP) is most efficient within the first 20 minutes. Based on these findings, a reaction time of 20 minutes was determined to be ideal for maximizing both the sensitivity and reliability of the detection assay.

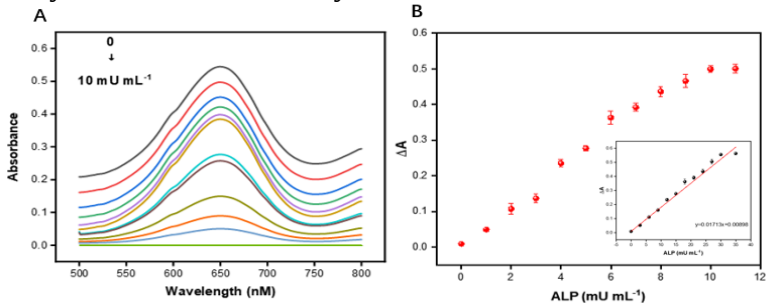

Figure 6: Linear range exploration

As ALP concentrations increased from 0 mU/mL to 10 mU/mL in Figure 6, there was a progressive fading of the blue oxTMB solution to a colorless and transparent state, corresponding to a decrease in absorbance at 652 nm (ΔA652 nm). For ALP concentrations ranging from 0.5 mU/mL to 10 mU/mL, a robust linear correlation was observed between ΔA652 nm and ALP concentration, given by the equation ΔA652 nm = 0.04962[ALP] + 0.009, with an R^2 value of 0.995. The detection limit for ALP was determined to be 0.091 mU/mL, based on a signal-to-noise ratio of 3. These results underscore the method's broad linear dynamic range and high sensitivity for the detection of both AA and ALP.

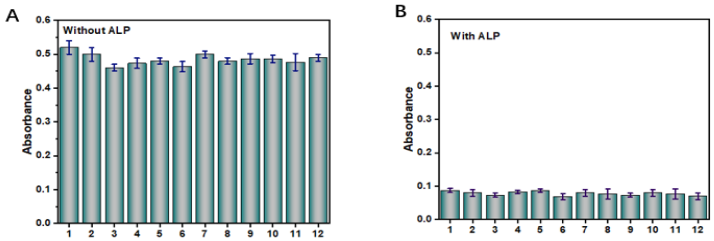

Figure 7: Verification of anti-interference

To appraise the sensor system's resilience against interference, an assessment was conducted on the influence of ubiquitous cations including sodium (Na^+), potassium (K^+), and calcium (Ca^{2+}), as well as anionic species such as chloride (Cl^-) and nitrate (NO_3^-). Additionally, the impact of amino acids—alanine (Ala), cysteine (Cys), and glutamic acid (Glu)—and a spectrum of biomolecules like bovine serum albumin (BSA), ovalbumin (OVA), tryptophan (Try), pancreatin (Pan), and pepsin (Pep) was scrutinized. Figure 7 delineates these assessments. The experimental outcomes evinced a marginal effect on the absorbance measurements at 652 nm (ΔA652 nm) when these interferents were present, attesting to the sensor's superior selectivity. Intriguingly, the absorbance alterations in the presence of ALP and the aforementioned interferents were congruent with those observed for

ALP in isolation. This congruence affirms the sensor's high specificity for detecting ALP-mediated hydrolysis of AA2P, devoid of interference from extraneous proteins or enzymatic activities.

4. Conclusion

In summary, the Fe_3O_4@MIL@Pt nanocomposite material exhibits remarkable catalytic surface properties, highlighting its exceptional catalytic efficiency. This study introduces a novel triple signal amplification technique that significantly enhances the precise detection of ascorbic acid (AA) and alkaline phosphatase (ALP) activity. The Fe_3O_4@MIL@Pt nanocomposite, with its optimized design, not only maximizes the individual benefits of each component but also leverages their synergistic interactions to optimize colorimetric analysis. This advancement provides new insights into ALP activity detection and expands the applications of enzyme-linked immunosorbent assays (ELISA) for ALP, demonstrating great potential for practical applications in various fields.

References

[1] MILLÁN J L. Purinerg. Signal. , 2006, 2(2): 335.

[2] F.Y. Zheng, S.H. Guo, F. Zeng, J. Li, S.Z. Wu, Ratiometric fluorescent probe for alkaline phosphatase based on betaine-modified polyethylenimine via excimer/monomer conversion, Anal. Chem. 86 (2014) 9873–9879.

[3] G.L. Li, H.L. Fu, X.J. Chen, P.W. Gong, G. Chen, L. Xia, H. Wang, J.M. You, Y.N. Wu,Facile and sensitive fluorescence sensing of alkaline phosphatase activity with photoluminescent carbon dots based on inner filter effect, Anal. Chem. 88 (2016), 2720–2726.

[4] D.W. Yang, Z.Z. Guo, Y.G. Tang, P. Miao, Poly(thymine)-templated selective formation of copper nanoparticles for alkaline phosphatase analysis aided by alkyneazide cycloaddition "click" reaction, ACS Appl. Nano Mater. 1 (2018) 168–174.

[5] X. Niu, K. Ye, L. Wang, Y. Lin, D. Du, A review on emerging principles and strategies for colorimetric and fluorescent detection of alkaline phosphatase activity, Anal. Chim. Acta 1086 (2019) 29–45.

[6] S.M. Shaban, S. Byeok Jo, E. Hafez, J. Ho Cho, D.-H. Kim, A comprehensive overview on alkaline phosphatase targeting and reporting assays, Coord. Chem. Rev. 465 (2022) 214567.

[7] T. Balbaied, A. Hogan, E. Moore, Electrochemical detection and capillary electrophoresis: comparative studies for alkaline phosphatase (ALP) release from living cells, Biosensors (Basel) 10 (8) (2020), https://doi.org/10.3390/bios10080095.

[8] Y. Liu, E. Xiong, X. Li, J. Li, X. Zhang, J. Chen, Sensitive electrochemical assay of alkaline phosphatase activity based on TdT-mediated hemin/G-quadruplex DNAzyme nanowires for signal amplification, Biosens. Bioelectron. 87 (2017) 970–975, https://doi.org/10.1016/j.bios.2016.09.069.

[9] S. Li, J. Li, B. Geng, X. Yang, Z. Song, Z. Li, B. Ding, J. Zhang, W. Lin, M. Yan, TPE based electrochemiluminescence for ALP selective rapid one-step detection applied in vitro, Microchem. J. 164 (2021), https://doi.org/10.1016/j. microc.2021.106041.

[10] H. Jiang, X. Wang, Alkaline phosphatase-responsive anodic electrochemiluminescence of CdSe nanoparticles, Anal. Chem. 84 (16) (2012) 6986–6993, https://doi.org/10.1021/ac300983t.

[11] J. Dong, Y. Li, M. Zhang, Z. Li, T. Yan, W. Qian, Ultrasensitive surface-enhanced Raman scattering detection of alkaline phosphatase, Anal. Methods 6 (22) (2014) 9168–9172, https://doi.org/10.1039/c4ay01885k.

[12] Y. Zeng, J.-Q. Ren, S.-K. Wang, J.-M. Mai, B. Qu, Y. Zhang, A.-G. Shen, J.-M. Hu,Rapid and reliable detection of alkaline phosphatase by a hot spots amplification strategy based on well-controlled assembly on single nanoparticle, ACS Appl. Mater. Interfaces. 9 (35) (2017) 29547–29553, https://doi.org/10.1021/acsami.7b09336.

[13] Q. Yang, X. Wang, H. Peng, M. Arabi, J. Li, H. Xiong, J. Choo, L. Chen, Ratiometric fluorescence and colorimetry dual-mode assay based on manganese dioxide nanosheets for visual detection of alkaline phosphatase activity, Sens. Actuators B Chem. 302 (2020), https://doi.org/10.1016/j.snb.2019.127176.

[14] I. Apostol, R. Kuciel, E. Wasylewska, W.S. Ostrowski, Phosphotyrosine as a substrate of acid and alkaline phosphatases, Acta Biochim. Pol. 32 (3) (1985) 187–197.

[15] P.J. Stankiewicz, M.J. Gresser, Inhibition of phosphatase and sulfatase by transition-state analogues, Biochemistry 27 (1) (1988) 206–212.

[16] J. Wang, Q. Lu, C. Weng, X. Li, X. Yan, W. Yang, B. Li, X. Zhou, Label-free colorimetric detection of acid phosphatase and screening of its inhibitors based on biomimetic oxidase activity of MnO2 nanosheets, ACS Biomater. Sci. Eng. 6 (5) (2020) 3132–3138, https://doi.org/10.1021/acsbiomaterials.0c00217.

[17] L. Dong, Q. Miao, Z. Hai, Y. Yuan, G. Liang, Enzymatic hydrogelation-induced fluorescence turn-off for sensing alkaline phosphatase in vitro and in living cells, Anal. Chem. 87 (13) (2015) 6475–6478, https://doi.org/10.1021/acs. analchem.5b01657.
[18] F. Zheng, S. Guo, F. Zeng, J. Li, S. Wu, Ratiometric fluorescent probe for alkaline phosphatase based on betaine-modified polyethylenimine via excimer/monomer conversion, Anal. Chem. 86 (19) (2014) 9873–9879, https://doi.org/10.1021/ac502500e.
[19] Y.H. Lin, J.S. Ren, X.G. Qu, Nano-gold as artificial enzymes: hidden talents, Adv.Mater. 26 (2014) 4200–4217.
[20] Y.H. Lin, J.S. Ren, X.G. Qu, Catalytically active nanomaterials: a promising candidate for artificial enzymes, Acc. Chem. Res. 47 (2014) 1097–1105.
[21] H. Wei, E.K. Wang, Nanomaterials with enzyme-like characteristics (nanozymes):next-generation artificial enzymes, Chem. Soc. Rev. 42 (2013) 6060–6093.
[22] J.J.X. Wu, X.Y. Wang, Q. Wang, Z.P. Lou, S.R. Li, Y.Y. Zhu, L. Qin, H. Wei, Nanomaterials with enzyme-like characteristics (nanozymes): next-generation artificial enzymes (II), Chem. Soc. Rev. 48 (2019) 1004–1076.
[23] A. Asati, S. Santra, C. Kaittanis, S. Nath, J.M. Perez, Oxidase-like activity of polymer-coated cerium oxide nanoparticles, Angew. Chem., Int. Ed. 48 (2009) 2308–2312.
[24] H.H. Deng, X.L. Lin, Y.H. Liu, K.L. Li, Q.Q. Zhuang, H.P. Peng, A.L. Liu, X.H. Xia, W. Chen, Chitosan-stabilized platinum nanoparticles as effective oxidase mimics for colorimetric detection of acid phosphatase, Nanoscale 9 (2017) 10292–10300.
[25] B. Liu, Z. Huang, J. Liu, Boosting the oxidase mimicking activity of nanoceria by fluoride capping: rivaling protein enzymes and ultrasensitive F− detection, Nanoscale 8 (2016) 13562–13567.
[26]Chen, H.; Qiu, Q.; Sharif, S.; Ying, S.; Wang, Y.; Ying, Y.Solution-Phase Synthesis of Platinum Nanoparticle-Decorated MetalOrganic Framework Hybrid Nanomaterials as Biomimetic Nanoenzymes for Biosensing Applications. ACS Appl. Mater. Interfaces 2018, 10, 24108−24115.
[27] D. Wei, D. Xiong, N. Zhu, Y. Wang, X. Hu, B. Zhao, J. Zhou, D. Yin, Z. Zhang, Copper peroxide nanodots encapsulated in a metal–organic framework for selfsupplying hydrogen peroxide and signal amplification of the dual-mode immunoassay, Anal. Chem. 94 (38) (2022) 12981–12989.
[28] Q. Wang, X. Wang, H. Wei, Spinel-oxide-based laccase mimics for the identification and differentiation of phenolic pollutants, Anal. Chem. 94 (28) (2022) 10198–10205.
[29] Z. Xu, Z. Qiu, Q. Liu, Y. Huang, D. Li, X. Shen, K. Fan, J. Xi, Y. Gu, Y. Tang, J. Jiang,J. Xu, J. He, X. Gao, Y. Liu, H. Koo, X. Yan, L. Gao, Converting organosulfur compounds to inorganic polysulfides against resistant bacterial infections, Nat. Commun. 9 (1) (2018) 3713.
[30] Y. Shen, X. Gao, H. Chen, Y. Wei, H. Yang, Y. Gu, Ultrathin C3N4 nanosheets-based oxidase-like 2D fluorescence nanozyme for dual-mode detection of organophosphorus pesticides, J. Hazard Mater. 451 (2023) 131171.
[31] T. Lin, Y. Qin, Y. Huang, R. Yang, L. Hou, F. Ye, S. Zhao, A label-free fluorescence assay for hydrogen peroxide and glucose based on the bifunctional MIL-53(Fe) nanozyme, Chem. Commun. 54 (14) (2018) 1762–1765.
[32] Emir, G.; Dilgin, Y.; Ramanaviciene, A.; Ramanavicius, A.Microchem. J. 2021, 161, 105751.
[33] H. Wei, E. Wang, Nanomaterials with enzyme-like characteristics (nanozymes): next-generation artificial enzymes, Chem. Soc. Rev. 42 (14) (2013) 6060–6093.
[34] Gao Z, Xu M, Lu M, Chen G and Tang D, Urchin-like (gold core)@(platinum shell) nanohybrids: a highly efficient peroxidase-mimetic system for in situ amplified colorimetric immunoassay. Biosens Bioelectron 70:194–201 (2015).
[35] Ren R, Cai G, Yu Z, Zeng Y and Tang D, Metal-polydopamine framework: an innovative signal-generation tag for colorimetric immunoassay. Anal Chem 90:11099–11105 (2018).
[36] Gao Z, Lv S, Xu M and Tang D, High-index {hk0} faceted platinum concave nanocubes with enhanced peroxidase-like activity for an ultrasensitive colorimetric immunoassay of the human prostate-specificantigen. Analyst 142:911–917 (2017).